

# Centre-of-momentum Variables in $\nu_\mu\text{CC}1\text{p}1\pi$

Weijun Li<sup>1</sup>

<sup>1</sup>*University of Oxford, Dept. of Physics, Oxford OX1 3RH, UK\**

(Dated: January 16, 2025)

This study introduces a novel set of variables designed to isolate final-state interactions (FSI) from the effects of nuclear initial states (IS). Through detailed simulation studies, this work demonstrates the ability of these variables to distinguish FSI contributions with minimal dependence on IS, highlighting their potential for advancing neutrino interaction modeling.

## I. INTRODUCTION

Significant efforts have been devoted to measuring Charge-Parity (CP) violation in the neutrino sector through long-baseline (LBL) experiments. In these experiments, CP violation is quantified by the difference between neutrino oscillation and anti-neutrino oscillation. LBL experiments quantify  $\delta_{\text{CP}}$  by comparing the energy spectra of  $\nu_e$  and  $\bar{\nu}_e$  oscillated from  $\nu_\mu$  and  $\bar{\nu}_\mu$ , respectively. There are two major challenges to this measurement. Firstly, the far detector of an LBL experiment is by design hundreds of kilometres away from the neutrino source, which unavoidably lead to low statistics. Secondly, as the energy of each incoming neutrino is unknown and thus the type of the individual neutrino bound-nucleon interaction is also unknown, oscillation predictions have to take the form of energy spectra for a chosen final state topology.

Large-scale experiments, such as Hyper-Kamiokande [1] and the Deep Underground Neutrino Experiment (DUNE) [2–6], address the first challenge by constructing gigantic far detectors to increase event rates. To match the reduction of statistical uncertainties, it is critical to develop advanced neutrino-nucleus interaction models or to better constrain existing ones to minimize the systematic uncertainties arisen from the second challenge. The neutrino-nucleus interaction is a convolution of multiple processes: the nucleon initial state (IS), the neutrino-nucleon interaction, and final state interactions (FSI). In particular, due to FSI, an event topology, e.g.  $\text{CC}0\pi$ , does not correspond only to a type of neutrino-nucleon interaction, e.g. quasi-elastic like, but also contains contribution from other interactions such as resonance production, because FSI could produce or absorb additional pions. Thus, accurate  $\delta_{\text{CP}}$  measurements depend heavily on neutrino interaction models estimating contributions of different neutrino-nucleon interactions to final-state topologies [7].

To better understand the complex neutrino-nucleus interactions, new or upgraded experiments with sophisticated detectors have commenced to explore a larger interaction kinematic phase space and to collect a significantly larger amount of data. For instance, the Tokai-to-Kamioka (T2K) experiment [8] has upgraded its near

detector (ND) and started data collection in June 2024. The Super Fine-Grain Detector (SFGD), part of the T2K ND upgrade [9], provides improved proton detection with lower thresholds, higher resolution, and greater efficiency. Meanwhile, the Short-baseline Near Detector (SBND) [10] has also begun operations in 2024. It is a new LArTPC with an active mass of 112 ton placed at 110 m from the neutrino source. Due to its large active mass and proximity to the source, it is expected to collect a huge number of neutrino interaction events each year. On one hand, the expanded kinematic phase space allows for measuring new variables. On the other, the influx of high-quality data offers an ideal testing ground for novel measurement techniques. Taking advantage of these advancements, it is timely to explore new ideas involving pions in the final states, given the broad energy spectrum of the DUNE beamline, which includes substantial contributions from resonance production comparable to quasi-elastic interactions,

One effective method of utilizing the near detector data is to constrain model parameters through tuning. Successful examples [11–13] have shown improved data-Monte Carlo (MC) agreement after tuning existing models using various combinations of measurements from different experiments. One difficulty of tuning is that many variables are affected by all processes of the complicated neutrino-nucleus interaction, making it both challenging to study the different models in isolation and numerically expensive and cumbersome to tune all processes at once. Nuclear effects, such as IS and FSI, occur within the nucleus and remain unobservable with current detectors, making them a major source of systematic uncertainties. Cleverly constructed variables, such as Transverse Kinematic Imbalance (TKI) [14, 15] or Generalized Kinematic Imbalance (GKI) [16], are sensitive to nuclear effects, and past measurements have successfully constrained models [17]. While TKI is sensitive to both IS and FSI, except  $\delta\alpha_{\text{T}}$ , which is predominantly sensitive to FSI but is affected by small uncertainties in the neutrino direction, new variables like  $p_{\text{long}}$  [18] are designed to be sensitive to specific nuclear effects, such as the removal energy.

Having more specialized measurements, like  $p_{\text{long}}$ , can further fine-tune our models, especially in light of the improved detection capabilities. This work proposes a new set of variables, called center-of-momentum (COM) variables, for charge current single pion single proton ( $\text{CC}1\pi 1\text{p}$ ) events, timely for the increasingly precise mea-

\* weijun.li@physics.ox.ac.uk

measurements with pions in the final states COM variables enable more focused studies of FSI by differentiating between FSI models independently of IS models.

This paper will elaborate on the concept of the COM variables and present MC analysis results focusing on the COM angle and demonstrating its ability to distinguish FSI models and its independence from IS.

## II. THE COM VARIABLES

When a neutrino has sufficient energy, it can excite a nucleon into a resonance state, for example the  $\Delta^{++}$ . This process is referred to as a resonance (RES) interaction. Since  $\Delta^{++}(1232)$ , simply referred to as  $\Delta^{++}$  unless stated otherwise, is one of the most commonly observed resonances in neutrino experiments, this work focuses on it as an example. Nevertheless, the concept presented here is equally applicable to other resonances, and the methodology can be easily generalized.

The resonance decays rapidly, before leaving the nucleus, via the process



In the  $\Delta^{++}$  rest frame, as illustrated on the top left in Fig. 1, the kinematics of this two-body decay are well-defined and the proton and pion are emitted back-to-back. The pion decay angle,  $\theta_{\pi\Delta}$ , is defined as the angle between  $\vec{p}_{\pi}^{(0)}$  and the  $x$ -axis, which is taken to align with  $\vec{p}_{\Delta}$ , the momentum of  $\Delta^{++}$  in the lab frame.  $\theta_{\pi\Delta}$  is a resonance property that follows an underlying distribution defined by various models [19–22].

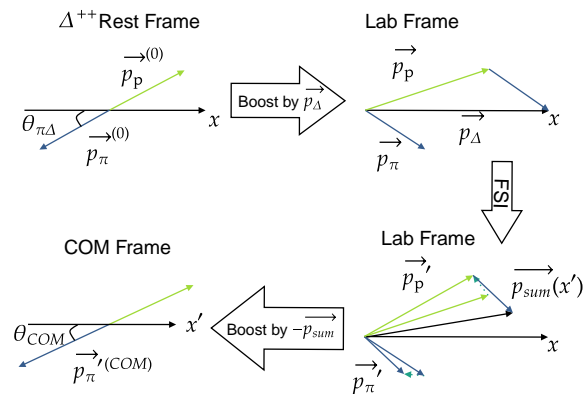


FIG. 1: Schematic illustration of the COM angle.

Without FSI,  $\vec{p}_{\text{sum}} = \vec{p}_{\Delta}$  and the lab frame and the  $\Delta^{++}$  rest frame can be transformed into each other by  $\vec{p}_{\Delta}$ . With FSI,  $\vec{p}_{\text{sum}} \neq \vec{p}_{\Delta}$ , the  $\Delta^{++}$  rest frame is not accessible, but the lab frame can be boosted into the COM frame using  $\vec{p}_{\text{sum}}$ . Hence, the major difference of the COM frame from the  $\Delta^{++}$  rest frame is caused by FSI.

The kinematics in the lab frame are related to those in the  $\Delta^{++}$  rest frame by a boost with  $\vec{p}_{\Delta}$ , as depicted on the top right of Fig. 1. Without FSI,  $\vec{p}_{\Delta}$  equals the sum of  $\vec{p}_p$  and  $\vec{p}_{\pi}$ . However, the target materials of modern day detectors are mainly comprised of nucleus with multiple nucleons and FSI alters the kinematics of the hadrons considerably, as illustrated by the dotted arrows in the bottom right of Fig. 1.

The altered momenta,  $\vec{p}'_p$  and  $\vec{p}'_{\pi}$ , are the ones measured by detectors. Their sum generally differs from  $\vec{p}_{\Delta}$ . Thus, the  $\Delta^{++}$  rest frame with its simple kinematic relations becomes inaccessible. Nevertheless, the system can be boosted to the proton-pion COM frame using  $\vec{p}_{\text{sum}}$ , as depicted in the bottom left of Fig. 1, where the  $x'$ -axis is taken to align with the  $\vec{p}_{\text{sum}}$  direction in the lab frame. Similarly, a pion decay angle,  $\theta_{\text{COM}}$ , can be defined between,  $\vec{p}_{\pi}^{(\text{COM})}$ , the pion momentum in the COM frame, and the  $x'$ -axis. Due to FSI,  $\theta_{\text{COM}}$  typically differs from  $\theta_{\pi\Delta}$ .

The COM frame coincides with the  $\Delta^{++}$  rest frame only in the absence of FSI. Thus, the strength of FSI dictates the deviation of  $\theta_{\text{COM}}$  from  $\theta_{\pi\Delta}$ . In practice, the measured  $\theta_{\text{COM}}$  serves as a probe for studying FSI.  $\theta_{\pi\Delta}$ , being a rest-frame property of  $\Delta^{++}$ , is independent of the resonance's momentum, neutrino energy, and IS. In neutrino event generators,  $\theta_{\text{COM}}$  deviates from  $\theta_{\pi\Delta}$  only due to FSI, which is independent of neutrino energy and IS. Therefore,  $\theta_{\text{COM}}$  retains these important independencies. As different resonances could have different decay properties,  $\theta_{\pi R}$ , the similarly defined pion decay angle of a higher resonance,  $R$ , generally differs from  $\theta_{\pi\Delta}$ . Hence,  $\theta_{\text{COM}}$ , a superposition of  $\theta_{\pi\Delta}$  and all possible  $\theta_{\pi R}$ , will deviate from  $\theta_{\pi\Delta}$ , when more resonances become energetically possible with an increase in neutrino energy. This deviation will be further elaborated in the Sec. IV.

Moreover, the total energy in the COM frame will be equal to the mass of the resonance in the absence of FSI. Cutting on events with total energy far from the rest mass peak of the resonance will select events with minimal FSI effects, such as the  $\nu$ -H events. However, this work will focus on the COM angle only, and analysis on the total energy will be conducted in future works.

Up to this point, the discussion of resonance decay has been entirely general and can thus be applied to and validated by various experiments, including hadron scattering measurements. However, there are features specific to neutrino experiments. First, the resonance is generated through neutrino-nucleon interactions, which involve both vector and axial currents. Second, the interaction occurs within the nuclear medium. This work focuses on the latter, with the application of COM variables to the former reserved for future research.

While the COM angle may appear conceptually similar to the reconstructed Adler angle,  $\theta_{\text{Adt}}$ , in neutrino experiments [23], there are significant differences. Notably, the COM frame is reconstructed exclusively from hadronic kinematics, whereas the reconstructed Adler frame relies on leptonic kinematics and assumes stationary nucle-

ons. Consequently, the reconstruction of the Adler frame is implicitly influenced by IS effects, whereas the COM frame’s hadronic variables are impacted by final state interactions (FSI). Therefore,  $\theta_{\text{Adt}}$ , being a hadronic variable in the Adler frame, is influenced by both IS and FSI. Additionally, the necessity of reconstructing the neutrino energy renders  $\theta_{\text{Adt}}$  sensitive to neutrino flux uncertainties, which are among the largest systematic uncertainties in neutrino measurements [24–28].

### III. ANALYSIS RESULT

In the absence of existing measurements of the COM angle, MC studies were conducted to evaluate its potential advantages. MC samples were generated using GENIE [29, 30] for the T2K beam and target. Several GENIE tunes were compared, with the model details for each tune summarized in Table I. Each sample consists of 600,000 muon neutrino events, and a selection of charge current single pion and single proton ( $\nu_{\mu}\text{CC}1\pi 1p$ ) events was used to generate the plots.

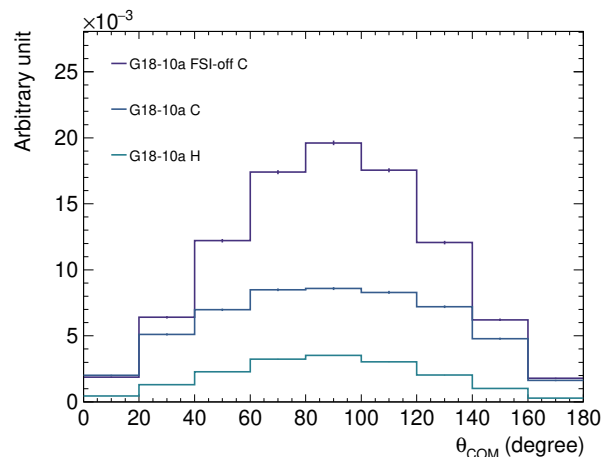
CMC	IS	QE	2p2h	RES	FSI
G18_01a_02_11b	RFG	LS	Dytman	RS	hA
G18_02a_02_11b	RFG	LS	Dytman	BS	hA
G18_10a_02_11b <sup>a</sup>	CFG	Valencia	Nieves	BS	hA
G18_10b_02_11b	LFG	Valencia	Nieves	BS	hN
G24_20i_00_000	SF-CFG	Valencia	SuSAv2	BS	hA
G24_20i_06_22c	SF-CFG	Valencia	SuSAv2	BS	hA(tuned)

<sup>a</sup> The GENIE default uses local Fermi gas instead.

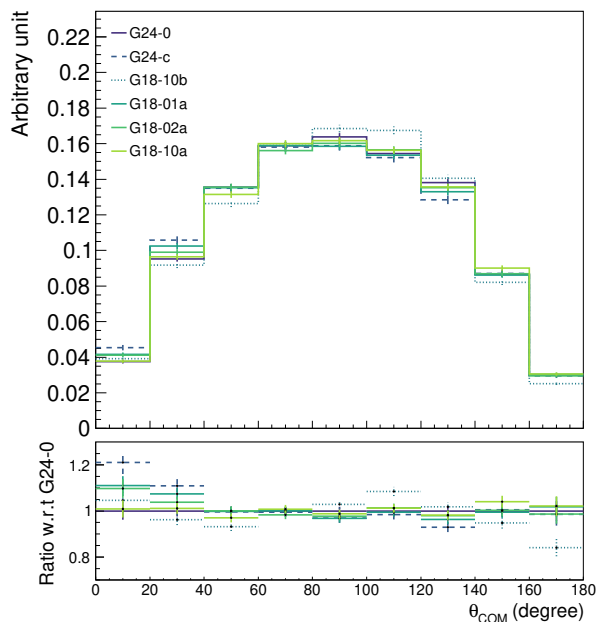
TABLE I: The four nuclear IS models are relativistic Fermi gas (RFG), local Fermi gas (LFG), correlated Fermi gas (CFG), spectral-function-like CFG (SF-CFG) [30–32]. The respective cross-section models are: 1) Quasielastic (QE) - Llewellyn-Smith (LS) [33] and Valencia [34]; 2) 2p2h - Dytman [35], Nieves [36] and SuSAv2 [37]; 3) RES - Rein-Sehgal [38] and Berger-Sehgal [39]. The FSI models are the built-in GENIE models [40], INTRANUKE hA and hN. Note that in G24\_20i\_06\_22c [17], the hA model has been tuned using TKI data, resulting in parameters that differ from the default hA.

As illustrated in Fig. 2 (a), enabling or disabling FSI has a significant effect on the  $\theta_{\text{COM}}$  cross-section as expected. More critically, Fig. 2 (b) shows that changing the underlying FSI model from hA (10a) to hN (10b) or from hA (10a) to hA (tuned, G24-c) results in a noticeable variation in the  $\theta_{\text{COM}}$  cross-section. In contrast, although numerous combinations of IS, QE, 2p2h, and RES models were tested, configurations using the hA FSI model produced nearly identical cross-sections. This demonstrates the potential of  $\theta_{\text{COM}}$  to distinguish between different FSI models, independent of many other factors.

To further examine the independence from IS of  $\theta_{\text{COM}}$ , the cross-section shape of  $\nu$ -C (with FSI on and off) is



(a) Cross-section normalized comparisons with FSI on/off for carbon and hydrogen with G18.10a\_02.11b.



(b) Area normalized comparisons for different tunes with FSI on for carbon.

FIG. 2:  $\theta_{\text{COM}}$  distribution comparisons using the T2K flux on different nuclei and with multiple GENIE configurations.

compared to that of  $\nu$ -H. The  $\nu$ -H interaction is free from any nuclear effects, while  $\nu$ -C without FSI reflects the impact of IS, including carbon removal energy and Fermi motion. When FSI is on, the full nuclear effects—both IS and FSI—are present. Fig. 3a shows that FSI has a substantial impact on the cross-section shape, as expected. The near overlap of the  $\nu$ -H and  $\nu$ -C (FSI-off) curves provides strong evidence for the proposed independence of  $\theta_{\text{COM}}$  from IS effects.

Although  $\theta_{\text{COM}}$  is conceptually similar to the recon-

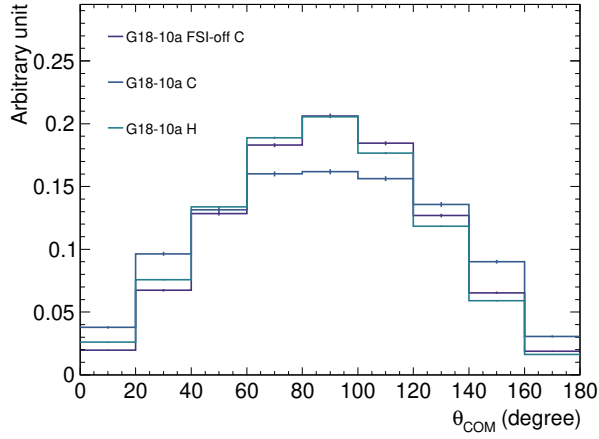
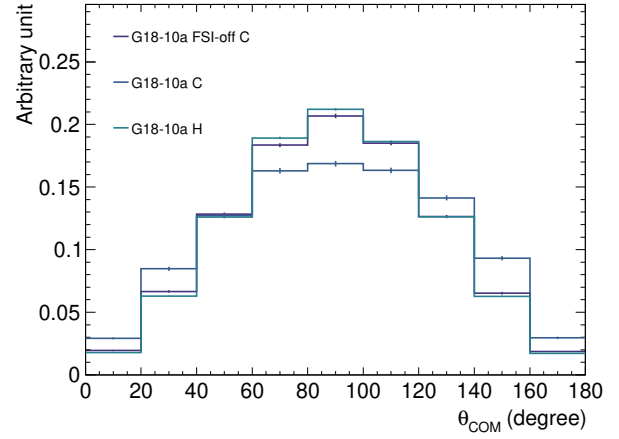
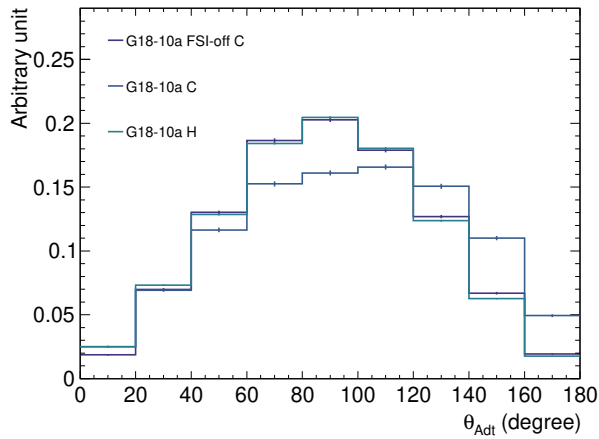
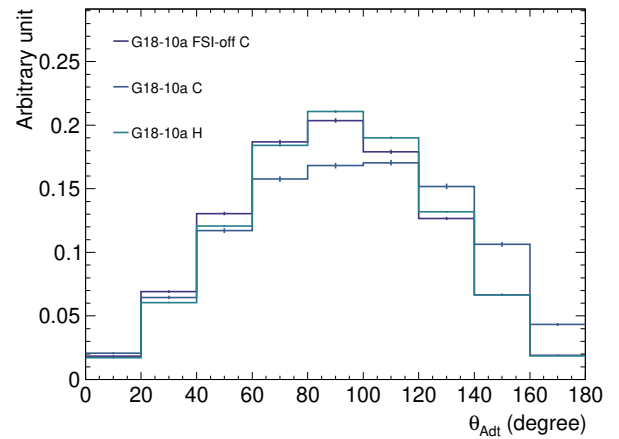
(a)  $\theta_{\text{COM}}$  - general  $\nu_{\mu}\text{CC}1\pi1\text{p}$ .(a)  $\theta_{\text{COM}}$  -  $\Delta^{++}$  decay.(b)  $\theta_{\text{Adt}}$  - general  $\nu_{\mu}\text{CC}1\pi1\text{p}$ .(b)  $\theta_{\text{Adt}}$  -  $\Delta^{++}$  decay.

FIG. 3: Area normalized comparisons for FSI on/off for carbon and hydrogen with G18\_10a\_02\_11b between  $\theta_{\text{COM}}$  and  $\theta_{\text{Adt}}$  using the T2K flux and target. with the bottom row has a more stringent selection to restrict the resonance to be  $\Delta^{++}$ .

FIG. 4: Area normalized comparisons between  $\theta_{\text{COM}}$  and  $\theta_{\text{Adt}}$  using the T2K flux and target. Comparing FSI on/off for carbon and hydrogen with G18\_10a\_02\_11b for  $\theta_{\text{COM}}$  (left)  $\theta_{\text{Adt}}$  (right), with the bottom row has a more stringent selection to restrict the resonance to be  $\Delta^{++}$ .

structured Adler angle,  $\theta_{\text{Adt}}$ , the latter is additionally influenced by IS effects. However, Fig. 3b suggests that the  $\nu$ -H and  $\nu$ -C (FSI-off) curves remain nearly as close as in Fig. 3a. When a stricter selection is made to select only events involving  $\Delta^{++}$  as shown in Fig. 4, the small difference in  $\theta_{\text{COM}}$  reduces further while the two curves deviate slightly more in  $\theta_{\text{Adt}}$ . This suggests that in the absence of FSI,  $\theta_{\text{COM}}$  could be a better construction of  $\theta$  than  $\theta_{\text{Adt}}$ .

Nevertheless, the small difference between the two curves for  $\theta_{\text{Adt}}$  indicates that despite IS dependence, IS does not significantly distort the shape of  $\theta_{\text{Adt}}$  appreciably. This observation could challenge the claimed IS independence of  $\theta_{\text{COM}}$ , as it might be due to the relatively minor influence of IS. To further examine this, a stress test was conducted by varying the removal energy of carbon across a wide range, even to unphysical levels,

to assess its effect on the shapes of  $\theta_{\text{COM}}$  and  $\theta_{\text{Adt}}$ . The results are presented in Fig. 5.

As seen in Fig. 5, variations in the removal energy ( $E_{\text{rm}}$ ) do not affect  $\theta_{\text{COM}}$  at all. In contrast, the  $\theta_{\text{Adt}}$  peak exhibits a noticeable shift, along with a gradual change in its shape. These results confirm that  $\theta_{\text{COM}}$  is independent of IS effects, while  $\theta_{\text{Adt}}$  exhibits IS dependence, as predicted.

Another important feature of  $\theta_{\text{COM}}$  is its independence from neutrino energy. Fig. 6 illustrates this behavior. The  $\theta_{\text{COM}}$  distribution shapes remain largely consistent for  $E_{\nu}$  values between 0.5 GeV and 2.0 GeV across most angles. However, deviations become more pronounced at smaller angles. As  $E_{\nu}$  increases to 5 GeV, a noticeable rise is observed in the small-angle region, likely due to the onset of a higher doubly positive resonance. If the anal-

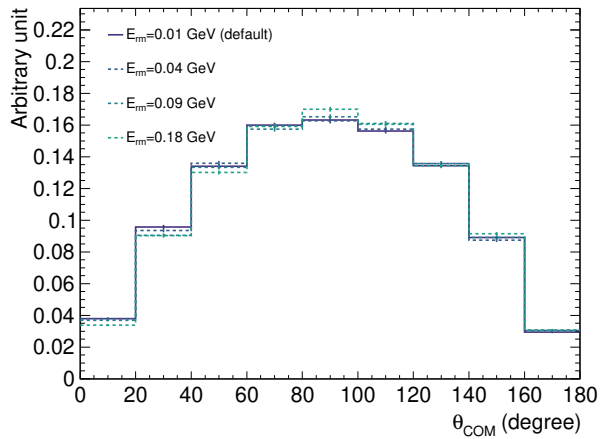
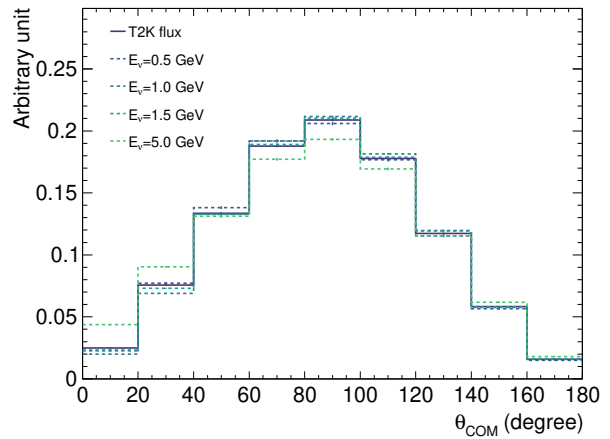
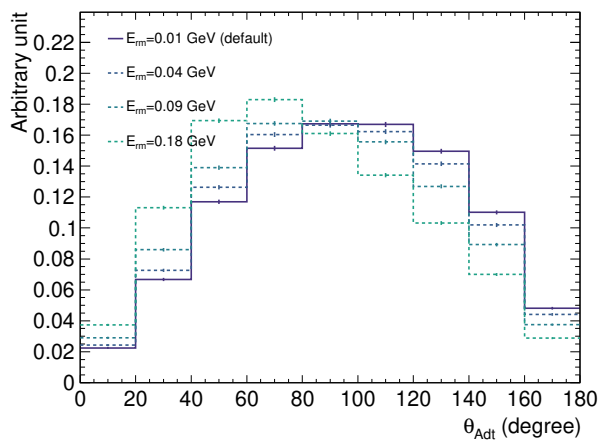
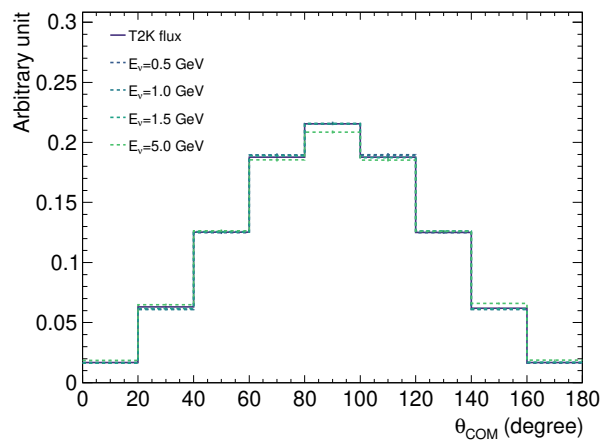
(a)  $\theta_{\text{COM}}$ (a)  $\nu_{\mu}\text{CC}1\pi1p$ (b)  $\theta_{\text{Adt}}$ (b)  $\Delta^{++}$  decay

FIG. 5: Area normalized comparisons for different removal energies,  $E_{\text{rm}}$ , with the T2K flux.

FIG. 6: Area normalized comparisons for different  $E_{\nu}$  fluxes for  $\theta_{\text{COM}}$ .

ysis is limited to  $\Delta^{++}$  as in Fig. 6(b), it is encouraging to observe that the different curves converge, confirming the independence of  $\theta_{\text{COM}}$  from  $E_{\nu}$ .

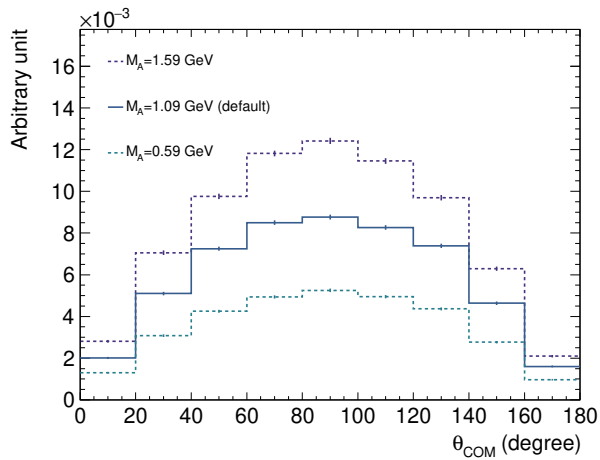
Besides  $E_{\nu}$ , another important component in the production of resonances is the part of the  $\nu$ -N interaction modeling that describes the resonance interaction. While  $\theta_{\text{COM}}$  for a single resonance is largely independent of how the resonance is produced unless there is a strong correlation between the production and decay of the resonance,  $\theta_{\text{COM}}$  will be affected by the composition of different resonances in the production process. As different resonances can have different decay angular distributions and  $\theta_{\text{COM}}$  does not distinguish between resonances that have the same decay channel, different combinations of resonances in production modelling will change the  $\theta_{\text{COM}}$  distribution. As a proxy to investigate the impact of a change in the resonance production model, the axial mass parameter,  $M_A$ , was varied to an exaggerated and most likely unphysical extent and the effect is shown in Fig. 7. As anticipated, Fig. 7a demonstrates that varying  $M_A$

alters the cross-section. However, it is reassuring to observe that the shape of  $\theta_{\text{COM}}$  remains almost identical, as shown in Fig. 7b.

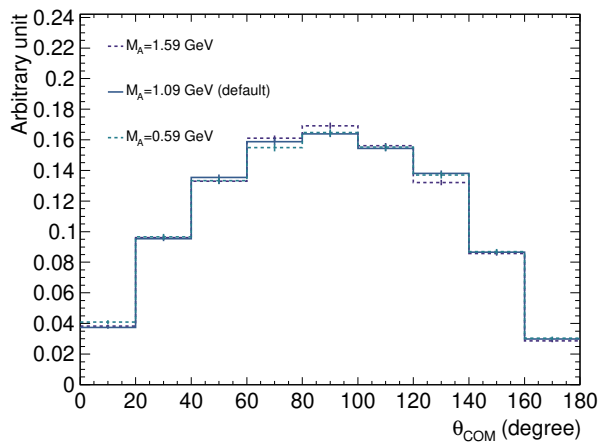
#### IV. DISCUSSION

The above simulation studies demonstrate that the COM angle is a novel variable with several advantages, and its measurement will be valuable for studying FSI independently of IS.

Although the analysis focus of  $\theta_{\text{COM}}$  is on nuclear effects, it is inherently affected by the resonance interaction modelling. Fortunately, the  $\nu$ -N interaction is relatively well-understood, particularly through direct studies of  $\nu$ -H interactions. As a result, future RES modeling is not expected to deviate drastically from current predictions, which are constrained by bubble chamber data. Even if the RES model were to change significantly, as explored in Fig. 7, the impact on the shape of  $\theta_{\text{COM}}$  remains min-



(a) cross section normalized



(b) area normalized

FIG. 7: Comparisons for different  $M_A$  values with the T2K flux.

imal, particularly for the T2K flux. This suggests that FSI models tuned using  $\theta_{\text{COM}}$ , e.g. following the methodology in Ref. [11], will continue to be applicable even if the RES model undergoes future updates, thereby enhancing the robustness of such FSI model tuning.

As noted in Sec. II, the  $\theta_{\text{COM}}$  distribution is influenced by the production of higher resonances that decay through the same channels as  $\Delta^{++}$ . The impact is two-fold. Firstly, due to general difference of  $\theta_{\pi\text{R}}$  from  $\theta_{\pi\Delta}$ ,  $\theta_{\text{COM}}$  would start to deviate from  $\theta_{\pi\Delta}$  (smeared by FSI), as shown in Fig. 6a. Although  $\theta_{\text{COM}}$  is inspired by  $\theta_{\pi\Delta}$ , it is not restricted to the reconstruction or estimation of  $\theta_{\pi\Delta}$ . Rather,  $\theta_{\text{COM}}$  by definition is the superposition of all energetically accessible  $\theta_{\pi\text{R}}$ , with  $\theta_{\pi\Delta}$  being the dominant component at low energy. If all  $\theta_{\pi\text{R}}$ 's are relatively well understood, a simple theoretically motivated expectation of  $\theta_{\text{COM}}$  can be obtained by adding the contributions from all possible R according to the relative production ratios. This simple approach is complicated by the second point - even with a complete understanding

of the FSI model, the predicted  $\theta_{\text{COM}}$  distribution would deviate from measurements due to correlations among different resonance production modes, i.e. the overall  $\theta_{\text{COM}}$  is not simply a linear combination of the individual  $\theta_{\pi\text{R}}$  contributions. Nevertheless, the influence of higher resonances is minor for low-energy neutrino beams and can be further reduced by applying an upper cut on the COM total energy, ensuring that the selected events predominantly arise from  $\Delta^{++}$  decay. Besides, even with higher resonance produced, such as  $\Delta(1600)$ , the decay to a proton and a single pion is no longer the dominant channel [41]. As FSI modeling improves and single-resonance models are refined through constraints from other experiments, the COM total energy cut could be lifted. This would enable the full  $\theta_{\text{COM}}$  distribution to be used for studying correlations and advancing RES modeling.

The sensitivity of the COM frame to FSI can be leveraged not only to study FSI but also to select events without FSI. These events are primarily composed of  $\nu$ -H interactions, which provide a unique opportunity for precise measurements of the axial current—a feature specific to neutrinos. Additionally, a  $\nu$ -H sample allows for the improvement of  $\nu$ -H modeling without the complications of IS and FSI, facilitating accurate neutrino energy reconstruction. These advantages have driven significant efforts to develop techniques for selecting a high-purity  $\nu$ -H sample, as seen in Ref. [14, 18, 42]. While Ref. [18] and Ref. [42] focuses on neutrino and antineutrino pion-less events respectively, Ref. [14] applies to the same event topology as the COM total energy. Preliminary studies have shown that applying a cut on COM energy can remove events with minimal transverse momentum imbalance, which could be combined with cuts on  $\delta p_{\text{TT}}$  and  $\delta p_{\text{T}}$  to create a high-purity  $\nu$ -H sample. This approach will be explored further in future studies.

Although the COM angle shares a similar reconstruction target with the Adler angle, there are key differences, as discussed in Sec. III. While these differences may appear minor, the conceptual distinction makes tuning the FSI model using the COM angle more adaptable to future developments. Furthermore, the analyses presented here are based on true information without any realistic fluctuations, meaning that challenges related to reconstruction—particularly those involving neutrino energy for the Adler angle—are not considered. Therefore, the full potential of the COM angle will be better realized in a cross-section measurement that accounts for these complexities.

## V. CONCLUSION

This study introduces a novel set of variables—the COM angle and total energy. These variables offer several advantageous properties, motivating their use in future cross-section measurements. These measurements have the potential to significantly improve our understanding and modeling of FSI processes in neutrino-

nucleus interactions, thereby contributing to more accurate neutrino cross-section predictions.

## VI. ACKNOWLEDGEMENT

The author would like to thank Stephen Dolan for his constructive advice and helpful discussion.

- 
- [1] K. Abe *et al.* (Hyper-Kamiokande), Hyper-Kamiokande Design Report, (2018), arXiv:1805.04163 [physics.ins-det].
- [2] R. Acciarri *et al.* (DUNE), Long-Baseline Neutrino Facility (LBNF) and Deep Underground Neutrino Experiment (DUNE): Conceptual Design Report, Volume 2: The Physics Program for DUNE at LBNF, (2015), arXiv:1512.06148 [physics.ins-det].
- [3] J. Strait *et al.* (DUNE), Long-Baseline Neutrino Facility (LBNF) and Deep Underground Neutrino Experiment (DUNE): Conceptual Design Report, Volume 3: Long-Baseline Neutrino Facility for DUNE June 24, 2015, (2016), arXiv:1601.05823 [physics.ins-det].
- [4] R. Acciarri *et al.* (DUNE), Long-Baseline Neutrino Facility (LBNF) and Deep Underground Neutrino Experiment (DUNE): Conceptual Design Report, Volume 1: The LBNF and DUNE Projects, (2016), arXiv:1601.05471 [physics.ins-det].
- [5] R. Acciarri *et al.* (DUNE), Long-Baseline Neutrino Facility (LBNF) and Deep Underground Neutrino Experiment (DUNE): Conceptual Design Report, Volume 4 The DUNE Detectors at LBNF, (2016), arXiv:1601.02984 [physics.ins-det].
- [6] V. Hewes *et al.* (DUNE), Deep Underground Neutrino Experiment (DUNE) Near Detector Conceptual Design Report, *Instruments* **5**, 31 (2021), arXiv:2103.13910 [physics.ins-det].
- [7] L. Alvarez-Ruso *et al.* (NuSTEC), NuSTEC White Paper: Status and challenges of neutrino–nucleus scattering, *Prog. Part. Nucl. Phys.* **100**, 1 (2018), arXiv:1706.03621 [hep-ph].
- [8] K. Abe *et al.* (T2K), The T2K Experiment, *Nucl. Instrum. Meth. A* **659**, 106 (2011), arXiv:1106.1238 [physics.ins-det].
- [9] K. Abe *et al.* (T2K), T2K ND280 Upgrade - Technical Design Report, (2019), arXiv:1901.03750 [physics.ins-det].
- [10] R. Acciarri *et al.* (MicroBooNE, LAr1-ND, ICARUS-WA104), A Proposal for a Three Detector Short-Baseline Neutrino Oscillation Program in the Fermilab Booster Neutrino Beam, (2015), arXiv:1503.01520 [physics.ins-det].
- [11] J. Tena-Vidal *et al.* (GENIE), Neutrino-nucleon cross-section model tuning in GENIE v3, *Phys. Rev. D* **104**, 072009 (2021), arXiv:2104.09179 [hep-ph].
- [12] J. Tena-Vidal *et al.* (GENIE), Hadronization model tuning in genie v3, *Phys. Rev. D* **105**, 012009 (2022), arXiv:2106.05884 [hep-ph].
- [13] J. Tena-Vidal *et al.* (GENIE), Neutrino-nucleus CC0 $\pi$  cross-section tuning in GENIE v3, *Phys. Rev. D* **106**, 112001 (2022), arXiv:2206.11050 [hep-ph].
- [14] X.-G. Lu, D. Coplowe, R. Shah, G. Barr, D. Wark, and A. Weber, Reconstruction of Energy Spectra of Neutrino Beams Independent of Nuclear Effects, *Phys. Rev. D* **92**, 051302 (2015), arXiv:1507.00967 [hep-ex].
- [15] X.-G. Lu, L. Pickering, S. Dolan, G. Barr, D. Coplowe, Y. Uchida, D. Wark, M. O. Wascko, A. Weber, and T. Yuan, Measurement of nuclear effects in neutrino interactions with minimal dependence on neutrino energy, *Phys. Rev.* **C94**, 015503 (2016), arXiv:1512.05748 [nucl-th].
- [16] P. Abratenko *et al.* (MicroBooNE), Measurement of nuclear effects in neutrino-argon interactions using generalized kinematic imbalance variables with the MicroBooNE detector, *Phys. Rev. D* **109**, 092007 (2024), arXiv:2310.06082 [nucl-ex].
- [17] W. Li *et al.* (GENIE), First combined tuning on transverse kinematic imbalance data with and without pion production constraints, *Phys. Rev. D* **110**, 072016 (2024), arXiv:2404.08510 [hep-ex].
- [18] N. Baudis, S. Dolan, D. Sgalaberna, S. Bolognesi, L. Munteanu, and T. Dieminger, Longitudinal kinematic imbalances in neutrino and antineutrino interactions for improved measurements of neutrino energy and the axial vector form factor, *Phys. Rev. D* **110**, 032019 (2024), arXiv:2310.15633 [hep-ph].
- [19] D. Rein, Angular Distribution in Neutrino Induced Single Pion Production Processes, *Z. Phys. C* **35**, 43 (1987).
- [20] M. Kabirnezhad, Single pion production in neutrino-nucleon Interactions, *Phys. Rev. D* **97**, 013002 (2018), arXiv:1711.02403 [hep-ph].
- [21] M. Kabirnezhad, Single pion production in electron-nucleon interactions, *Phys. Rev. D* **102**, 053009 (2020), arXiv:2006.13765 [hep-ph].
- [22] M. Kabirnezhad, Single-pion production in electron-proton interactions, *Phys. Rev. C* **107**, 025502 (2023), arXiv:2203.15594 [hep-ph].
- [23] F. Sánchez, Possibility of measuring Adler angles in charged current single pion neutrino-nucleus interactions, *Phys. Rev. D* **93**, 093015 (2016), arXiv:1511.00501 [hep-ex].
- [24] K. Abe *et al.* (T2K), Measurement of the muon neutrino charged-current single  $\pi^+$  production on hydrocarbon using the T2K off-axis near detector ND280, *Phys. Rev. D* **101**, 012007 (2020), arXiv:1909.03936 [hep-ex].
- [25] K. Abe *et al.* (T2K), First T2K measurement of transverse kinematic imbalance in the muon-neutrino charged-current single- $\pi^+$  production channel containing at least one proton, *Phys. Rev. D* **103**, 112009 (2021), arXiv:2102.03346 [hep-ex].
- [26] P. Abratenko *et al.* ((MicroBooNE Collaboration)\*, MicroBooNE), Measurement of the differential cross section

- for neutral pion production in charged-current muon neutrino interactions on argon with the MicroBooNE detector, *Phys. Rev. D* **110**, 092014 (2024), arXiv:2404.09949 [hep-ex].
- [27] M. A. Acero *et al.* (NOvA), Measurement of  $\nu\mu$  charged-current inclusive  $\pi^0$  production in the NOvA near detector, *Phys. Rev. D* **107**, 112008 (2023), arXiv:2306.04028 [hep-ex].
- [28] A. Bercellie *et al.* (MINERvA), Simultaneous Measurement of Muon Neutrino  $\nu\mu$  Charged-Current Single  $\pi^+$  Production in CH, C, H<sub>2</sub>O, Fe, and Pb Targets in MINERvA, *Phys. Rev. Lett.* **131**, 011801 (2023), arXiv:2209.07852 [hep-ex].
- [29] C. Andreopoulos *et al.*, The GENIE Neutrino Monte Carlo Generator, *Nucl. Instrum. Meth. A* **614**, 87 (2010), arXiv:0905.2517 [hep-ph].
- [30] L. Alvarez-Ruso *et al.* (GENIE), Recent highlights from GENIE v3, *Eur. Phys. J. ST* **230**, 4449 (2021), arXiv:2106.09381 [hep-ph].
- [31] L. Munteanu, (2022), nuInt, Seoul, KOREA, [Conference presentation].
- [32] L. Munteanu, Genie generator (2023), commit SHA:64135ac.
- [33] C. H. Llewellyn Smith, Neutrino Reactions at Accelerator Energies, *Phys. Rept.* **3**, 261 (1972).
- [34] J. Nieves, J. E. Amaro, and M. Valverde, Inclusive quasi-elastic neutrino reactions, *Phys. Rev. C* **70**, 055503 (2004), [Erratum: *Phys.Rev.C* 72, 019902 (2005)], arXiv:nucl-th/0408005.
- [35] Katori, Teppei, Meson exchange current (MEC) models in neutrino interaction generators, AIP Conference Proceedings **1663**, 030001 (2015), eprint: [https://pubs.aip.org/aip/acp/article-pdf/doi/10.1063/1.4919465/13101054/030001\\_1\\_online.pdf](https://pubs.aip.org/aip/acp/article-pdf/doi/10.1063/1.4919465/13101054/030001_1_online.pdf).
- [36] J. Nieves, I. Ruiz Simo, and M. J. Vicente Vacas, Inclusive Charged-Current Neutrino-Nucleus Reactions, *Phys. Rev. C* **83**, 045501 (2011), arXiv:1102.2777 [hep-ph].
- [37] R. González-Jiménez, G. D. Megias, M. B. Barbaro, J. A. Caballero, and T. W. Donnelly, Extensions of Superscaling from Relativistic Mean Field Theory: the SuSAv2 Model, *Phys. Rev. C* **90**, 035501 (2014), arXiv:1407.8346 [nucl-th].
- [38] D. Rein and L. M. Sehgal, Neutrino Excitation of Baryon Resonances and Single Pion Production, *Annals Phys.* **133**, 79 (1981).
- [39] C. Berger and L. M. Sehgal, Lepton mass effects in single pion production by neutrinos, *Phys. Rev. D* **76**, 113004 (2007), arXiv:0709.4378 [hep-ph].
- [40] C. Andreopoulos, C. Barry, S. Dytman, H. Gallagher, T. Golan, R. Hatcher, G. Perdue, and J. Yarba, The GENIE Neutrino Monte Carlo Generator: Physics and User Manual, (2015), arXiv:1510.05494 [hep-ph].
- [41] S. Navas *et al.* (Particle Data Group), Review of particle physics, *Phys. Rev. D* **110**, 030001 (2024).
- [42] T. Cai *et al.* (MINERvA), Measurement of the axial vector form factor from antineutrino-proton scattering, *Nature* **614**, 48 (2023).